A Chirp Scaling Approach for Processing Squint Mode SAR Data

G. W. DAVIDSON
I. G. CUMMING
M. R. ITO
University of British Columbia

Image formation from squint mode synthetic aperture radar (SAR) is limited by image degradations caused by neglecting the range-variant filtering required by secondary range compression (SRC). Introduced here is a nonlinear FM chirp scaling, an extension of the chirp scaling algorithm, as an efficient and accurate approach to range variant SRC. Two methods of implementing the approach are described. The nonlinear FM filtering method is more accurate but adds a filtering step to the chirp scaling algorithm, although the extra computation is less than that of a time domain residual compression filter. The nonlinear FM pulse method consists of changing the phase modulation of the transmitted pulse, thus avoiding an increase in computation. Simulations show both methods significantly improve resolution width and sidelobe level, compared with existing SAR processors for squint angles above 10 deg for L-band and 20 deg for C-band.

Manuscript received July 28, 1993; revised August 10, 1994 and January 13, 1995.

IEEE Log No. T-AES/32/1/00780.

This work was supported by the Natural Sciences and Engineering Research Council of Canada and the B.C. Science Council Scholarships.

Authors' current addresses: G. Davidson, German Aerospace Research Establishment (DLR), German Remote Sensing Center (DFD), 82234 Oberpfaffenhofen, Germany; I. Cumming and M. Ito, Department of Electrical Engineering, University of British Columbia, 2356 Main Mall, Vancouver, BC, Canada.

I. INTRODUCTION

Synthetic aperture radar (SAR) is a technique in which backscattered microwave pulses are collected by an airplane or satellite, and processed to form an image of the surface of the Earth [1]. The moving antenna footprint covers a strip on the surface, and hence this type of imaging is called strip-map SAR. The dimensions of the image are azimuth (along the flight track) and range (cross track). In conventional SAR, the antenna is pointed at nearly right angles to the flight path, or broadside. The angle by which the antenna may be pointed forward or backward of broadside is called the squint angle. In a mode of strip-map SAR imaging known as squint mode SAR, the squint angle can be as much as several tens of degrees. This has the potential to provide information about surface structure through the measurement of the azimuthal angle dependence of backscatter [2]. Squinting could also increase the flexibility with which a desired area on the surface is imaged within a single pass of the platform.

Image formation in squint mode SAR is limited by approximations in conventional processing algorithms, such as in the standard range-Doppler algorithm [3, 4], which cause degradations such as blurring and thus prevent the full resolution and quality of the image from being realized. The problem stems from higher order range-azimuth coupling terms in the phase of the SAR transfer function, which require compensation by a range filtering operation called secondary range compression (SRC) [5, 6]. Recent approaches, such as the squint imaging mode algorithm and the chirp scaling algorithm, provide more accurate SRC to accommodate moderate squint [7, 8]. However, at higher squint, the range dependence of SRC becomes significant, and this has been neglected in processing because of the difficulty of implementing the space-variant filtering step. As a result, the image is focussed at a reference range, while resolution broadening and sidelobe level increase toward the edges of the range swath, causing noticeable degradation in spaceborne SAR for squint angles above 10 deg for L-band and 20 deg for C-band. In some cases, range-variant processing can be accomplished by an interpolation in the two-dimensional frequency domain, although this is expensive since it must be done very accurately to avoid artifacts in the image [9]. Finally, in spotlight SAR, squint is accommodated by the polar format algorithm [10]. However, this assumes that a relatively small area is being imaged, making it unsuitable for efficient processing of strip-map SAR data [11].

We present an accurate and efficient approach for processing full swath, squint mode SAR data, which extends the useful squint angle for spaceborne strip-map SAR up to 35 deg for L-band and 50 deg for C-band. Our approach, called nonlinear FM chirp

scaling, is an extension of the recently developed chirp scaling algorithm. In chirp scaling, properties of linear FM pulses are used to achieve the range-variant signal shift required in processing, without the need of implementing an interpolator. This is done by simply multiplying uncompressed range lines by an appropriate phase function, so each pulse compresses to a desired location, such that the range dependence of the required signal shift is removed [8, 12–14]. In our approach, the chirp scaling technique is extended to achieve the effect of the range-variant filtering required in SRC. This is done by incorporating a small nonlinear FM component into the received range signal, which interacts with the phase function multiply to remove the range dependence of SRC. Then accurate processing can proceed in the two-dimensional frequency domain.

Two methods are proposed for incorporating the nonlinear FM component into the range signal. The first, called the nonlinear FM filtering method, adds a filtering step to the chirp scaling algorithm in order to introduce the nonlinear FM component into the signal before the phase function is applied. This method is more accurate, and does not depend on the transmitted pulse. The filtering step is implemented in the frequency domain, and at high squint the extra computation involved is about half of what would be required by an extra time-domain filter to compensate for the range-dependent SRC error. The second method is called the nonlinear FM pulse method. In this method a small approximation to the nonlinear FM component is made so that it can be incorporated directly into the transmitted pulse. Thus, the phase modulation of the transmitted pulse is used as a kind of preprocessing, allowing the range dependence of SRC to be accommodated without increasing the computation above that of the original chirp scaling algorithm. The computation of the original chirp scaling algorithm is comparable or less than that of the standard range-Doppler algorithm [14], so that the nonlinear FM chirp scaling approach provides an excellent performance/cost tradeoff. Also, in both methods, all processing steps are performed with only fast Fourier transform (FFT) and multiply operations, which are relatively simple to implement.

The performance of the new approach, compared with range-Doppler and the original chirp scaling algorithm, is determined by measurements on an image formed from simulated point scatterer data, such as resolution width, sidelobe level, registration, and phase. The high squint performance of the nonlinear FM filtering method approaches the theoretical limit, given the system bandwidth, while the approximation in the nonlinear FM pulse method causes a slight degradation at the highest squint. Both methods of nonlinear FM chirp scaling show significant improvement over existing SAR algorithms for squint angles above 10 deg for L-band and 20 deg for C-band.

Section II reviews the SAR signal and describes approximations in the range-Doppler and chirp scaling algorithms. Next, Section III derives more accurate chirp scaling parameters for a spaceborne SAR geometry. Then, Sections IV and V describe the nonlinear FM filtering method and nonlinear FM pulse method, respectively. Also, Section VI presents the simulation results comparing the new methods with the range-Doppler and original chirp scaling algorithms. Finally, Section VII gives the conclusions.

II. BACKGROUND

This section describes the notation and terminology for modeling the SAR signal and understanding SAR processing operations. Also, approximations in existing SAR algorithms are described briefly in order to understand the improvement with the new approach.

A. SAR Signal

SAR processing can be described by considering the signal received from a single point scatterer: the point scatterer response. This is a function of azimuth-time η, and range-time τ, and is dependent on the range position r of the scatterer. It is given by

$$s(\eta,\tau;r) = w(\eta-\eta_c)p\left[\tau-\frac{2R(\eta;r)}{c}\right] \times \exp\left[-j\frac{4\pi f_0 R(\eta;r)}{c}\right] \quad (1)$$

where the following definitions have been used: $w(\eta)$ is the weighting in azimuth from the antenna pattern, which is shifted due to squint by the beam center offset time η_c. The complex baseband representation of the transmitted pulse $p(\tau)$ is delayed by the round trip travel time. Here c is the speed of light, and $R(\eta;r)$ is the instantaneous range to the scatterer at range position r. This can be modeled by

$$R(\eta;r) = \sqrt{r^2 + v_e^2(r)\eta^2} \quad (2)$$

where $v_e(r)$ is a range dependent "effective platform velocity" that is used to account for an orbital geometry [9, 15]. Also, the complex exponential factor in (1) arises from the phase delay of the carrier, after coherent demodulation of the received signal, where f_0 is the carrier frequency. An example of a transmitted pulse is

$$p(\tau) = m(\tau)\exp(-j\pi K\tau^2), \quad (3)$$

which is a linear FM pulse of frequency rate, K and $m(\tau)$ is the pulse amplitude of duration T.

The range-dependent SAR transfer function is the two-dimensional Fourier transform of the point scatterer response, which can be shown to have the

form [16, 17]:

$$S_2(f_\eta, f_\tau; r) = P(f_\tau) W(f_\eta - f_{\eta c}) \exp[j\Phi(f_\eta, f_\tau; r)] \tag{4}$$

where f_τ is range-frequency and f_η is azimuth-frequency. Here $P(f_\tau)$ is the Fourier transform of the transmitted pulse, which for a linear FM pulse is

$$P(f_\tau) = M(f_\tau) \exp\left[j \frac{\pi f_\tau^2}{K}\right] \tag{5}$$

where $M(f_\tau)$ is the amplitude which determines the range bandwidth. Also, $W(f_\eta - f_{\eta c})$ is an amplitude weighting in azimuth-frequency due to the antenna pattern. This is centered on a value of azimuth-frequency called the Doppler centroid $f_{\eta c}$, which depends on the squint angle. The phase of the SAR transfer function $\Phi(f_\eta, f_\tau; r)$ is most important in SAR processing, since it must be matched accurately to focus the image. To facilitate the development of processing algorithms, this phase can be expressed as a series in f_τ:

$$\Phi(f_\eta, f_\tau; r) = \phi_0(f_\eta; r) + \phi_1(f_\eta; r) f_\tau + \phi_2(f_\eta; r) f_\tau^2 + \phi_3(f_\eta; r) f_\tau^3 + \cdots. \tag{6}$$

For moderate squint angles, only terms up to quadratic need to be included, whereas for higher squint the cubic term can become significant [18].

A representation of the point scatterer response in the range-time and azimuth-frequency (Doppler) domain provides a useful description of SAR processing operations for algorithms such as range-Doppler and chirp scaling. Assuming a linear FM pulse and keeping terms up to the quadratic in the phase expansion, a range inverse Fourier transform of the SAR transfer function gives the following range-Doppler form of the point scatterer response [17]:

$$S(f_\eta, \tau; r) = H_{ac}(f_\eta; r) m\left[\frac{K_m}{K}(\tau - \tau_d)\right] \times \exp[-j\pi K_m (\tau - \tau_d)^2]. \tag{7}$$

Here $H_{ac}(f_\eta; r)$ is the conjugate of the azimuth compression filter, corresponding to the first phase term in (6), which is independent of f_τ. This also includes the amplitude $W(f_\eta - f_{\eta c})$. Next, the signal delay in the range-Doppler domain $\tau_d(f_\eta; r)$ results from the linear phase term in the SAR transfer function. The variation of this delay with azimuth-frequency is called range migration, which must be removed during processing by range cell migration correction (RCMC), before azimuth compression can be performed. The shape of the range migration trajectory depends on the range r of the scatterer, and has the form

$$\tau_d(f_\eta; r) = \frac{2r}{c\gamma(f_\eta; r)} \tag{8}$$

where the factor γ is defined by

$$\gamma(f_\eta; r) = \sqrt{1 - \frac{c^2 f_\eta^2}{4 f_0^2 v_e^2(r)}}. \tag{9}$$

Finally, the frequency rate $K_m(f_\eta; r)$ is the result of combining the quadratic phase terms of the SAR transfer function from the linear FM pulse and the $\phi_2(f_\eta; r)$ term:

$$\frac{\pi}{K_m(f_\eta; r)} = \frac{\pi}{K} + \phi_2(f_\eta; r). \tag{10}$$

This frequency rate must be used to compress the signal in the range direction. The change in range-frequency rate from K to $K_m(f_\eta; r)$ is accommodated in processing by the SRC filter, which, without approximations, is dependent on azimuth-frequency and on range. An expression for $\phi_2(f_\eta; r)$ is given in the Appendix.

B. Approximations in SAR Algorithms

Squint performance of SAR processing algorithms is most affected by approximations to the modified range frequency rate $K_m(f_\eta; r)$. In the range-Doppler algorithm, which is most commonly used for processing spaceborne, strip-map SAR data, the range-frequency rate is approximated by its value at the Doppler centroid and at a reference range $K_m(f_{\eta c}; r_{\text{ref}})$. By ignoring the azimuth-frequency and range dependence of SRC, it can be performed efficiently by simply changing the frequency rate of the range matched filter. However, at even moderate squint angles (above about 5 deg for spaceborne L-band SAR), neglecting the azimuth-frequency dependence of SRC causes significant degradation throughout the image. In the chirp scaling algorithm, the SRC filter is allowed to vary with azimuth-frequency, by implementing it in the two-dimensional frequency domain, thus providing more accurate focusing. The range dependence of SRC is still neglected, however, so that the frequency rate is calculated at the reference range $K_m(f_\eta; r_{\text{ref}})$. At higher squint this results in image degradation that increases toward the edges of the range swath. Although the degradation could be alleviated by processing small range blocks, the amount of range migration at high squint requires a large overlap of blocks, making this inefficient. Also, to facilitate processing over the full swath, the range variation of the Doppler centroid is minimized in squint mode SAR by proper choice of the yaw and pitch angles of the antenna [7].

Another aspect of the range-Doppler algorithm is its use of an interpolator to perform range-dependent RCMC. This is relatively difficult to implement

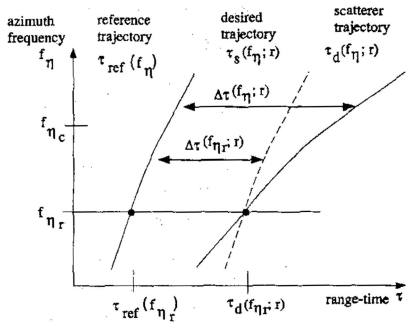

Fig. 1. Range migration trajectories in chirp scaling.

and is usually truncated for efficiency, introducing artifacts into the image. In chirp scaling algorithm, the interpolator for RCMC that is required in the range-Doppler algorithm is replaced by a phase function multiply, which is more efficient and avoids the issue of interpolator truncation.

III. DESIRED TRAJECTORY IN CHIRP SCALING

Chirp scaling uses the properties of phase modulated pulses to remove the range dependence of RCMC, so that the bulk of RCMC can be performed in the frequency domain. In extending the technique for processing high squint SAR data, it is desired to maintain the accuracy of RCMC. Because of the characteristics of SAR data at high squint in a spaceborne geometry, a more accurate formulation of the range dependence of RCMC is required.

In chirp scaling, the multiplication of uncompressed range signals by the phase function causes a range-dependent shift of the compressed pulses, resulting in a scaling of the range-time axis. By suitably choosing the scaling factors for range lines at each azimuth-frequency, the range migration trajectories for scatterers at all ranges can be made to have the same shape as the trajectory at a reference range. Thus the range dependence of the trajectories is removed. This is illustrated in Fig. 1, where $\tau_d(f_\eta;r)$ is a scatterer trajectory and $\tau_{\text{ref}}(f_\eta)$ is the reference trajectory. For a scatterer at range r, the desired trajectory which has the same shape as the reference trajectory is indicated by $\tau_s(f_\eta;r)$. The location of the desired trajectory is determined by the reference azimuth-frequency $f_{\eta r}$, which is where the scatterer trajectory and desired trajectory intersect [19, 20]. At each azimuth-frequency, let $\Delta\tau(f_\eta;r)$ be the range-time from the reference trajectory to the scatterer trajectory. The range-time from the reference trajectory to the desired trajectory is constant and equal to the value at $f_{\eta r}$, so the desired trajectory can be defined as

$$\tau_s(f_\eta;r) = \tau_{\text{ref}}(f_\eta) + \Delta\tau(f_{\eta r};r). \tag{11}$$

Thus, to achieve the desired trajectory, it is required to scale $\Delta\tau(f_\eta;r)$ to $\Delta\tau(f_{\eta r};r)$.

In the original derivation of the chirp scaling algorithm [8, 13], the desired trajectory is approximated by assuming a constant effective velocity parameter, so that

$$\tau_d(f_\eta;r) \approx \frac{2r}{c\gamma(f_\eta;r_{\text{ref}})}. \tag{12}$$

With this approximation, $\Delta\tau(f_\eta;r)$ and $\Delta\tau(f_{\eta r};r)$ are related linearly by the scale factor

$$\alpha(f_\eta) = \frac{\gamma(f_{\eta r};r_{\text{ref}})}{\gamma(f_\eta;r_{\text{ref}})} \tag{13}$$

so the desired trajectory is approximated by

$$\tau_s(f_\eta;r) \approx \tau_{\text{ref}}(f_\eta) + \frac{\Delta\tau(f_\eta;r)}{\alpha(f_\eta)}. \tag{14}$$

At high squint in a spaceborne geometry, the effect of the range-dependent effective velocity $v_e(r)$ must be taken into account in modeling the range dependence of RCMC. It has been demonstrated that accurate RCMC with chirp scaling can be performed in this case, by modifying the phase function [21]. To derive expressions for the chirp scaling parameters for this case, a more accurate representation of the desired trajectory is required. Since the effect of $v_e(r)$ on the range dependence of RCMC is small, it is sufficient to look for a higher order term in the approximation to the desired trajectory in (14). This is derived in the Appendix, with the result that the desired trajectory can be represented by

$$\tau_s(f_\eta;r) \approx \tau_{\text{ref}}(f_\eta) + \frac{\Delta\tau(f_\eta;r)}{\alpha_v(f_\eta)} + \beta(f_\eta)\Delta\tau^2(f_\eta;r) \tag{15}$$

where $\alpha_v(f_\eta)$ represents a linear scaling which has been modified slightly from the previous scale factor $\alpha(f_\eta)$, and $\beta(f_\eta)$ represents a nonlinear scaling to account for the nonlinear relationship between $\Delta\tau(f_\eta;r)$ and $\Delta\tau(f_{\eta r};r)$ in an orbital geometry. The expressions for the scale factors are given in the Appendix. These are used in the next section to ensure accurate RCMC with the nonlinear FM chirp scaling approach.

IV. NONLINEAR FM FILTERING METHOD

Accurate focusing of squint mode SAR data requires the accommodation of the range dependence of SRC. In this section we show how the technique of chirp scaling can be extended to remove the range dependence of SRC, as well as RCMC. This is done by incorporating a small nonlinear FM component in the received range signal, thus providing an extra degree of freedom in determining the phase of the SAR transfer function after chirp scaling. This section describes the more accurate method for implementing this approach, called the nonlinear FM filtering method.

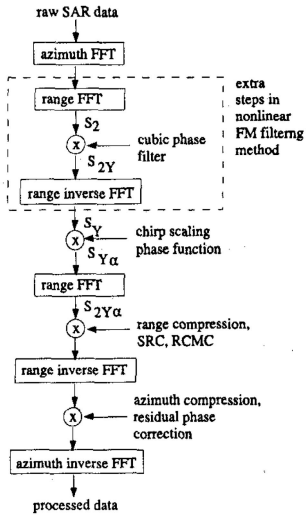

Fig. 2. Block diagram of nonlinear FM filtering method.

A. Description

A block diagram of the nonlinear FM filtering method is shown in Fig. 2. First, an azimuth FFT is taken of the SAR data. Then, at each azimuth-frequency, the nonlinear FM component is introduced to the range line by a range FFT, cubic phase filter multiply, and a range inverse FFT. This filtering step allows the nonlinear FM component to vary with azimuth-frequency, providing the most accurate accommodation of the range dependence of SRC. After the filtering step, processing continues as in the original chirp scaling algorithm. In the range-Doppler domain, each range line is multiplied by a phase function. Then a range FFT takes the data to the two-dimensional frequency domain, where a multiply performs the bulk RCMC and SRC. A range inverse transform takes the data back to the range-Doppler domain, where each azimuth line is multiplied by an azimuth compression filter which is augmented by a phase correction factor necessitated by chirp scaling. Finally, an azimuth inverse FFT produces the processed image.

To derive expressions for the cubic phase filter and chirp scaling phase function coefficients, consider the processing steps applied to the point scatterer response. After the azimuth FFT and range FFT, the signal is represented by the SAR transfer function in (4). The cubic phase filtering step is then represented by

$$S_{2Y}(f_\eta, f_\tau; r) = S_2(f_\eta, f_\tau; r) \exp\left[j \frac{2\pi}{3} Y(f_\eta) f_\tau^3 \right] \quad (16)$$

where $Y(f_\eta)$ is the azimuth-frequency varying cubic phase filter coefficient. As before, it is convenient to express the phase of the filtered SAR transfer function as a series in f_τ, where now the cubic phase term from (6), $\phi_3(f_\eta; r)$, is included. This term is still small enough that its range dependence can be neglected, and can be combined with the cubic phase filter coefficient to define the modified coefficient:

$$Y_m(f_\eta) = Y(f_\eta) + \frac{3}{2\pi} \phi_3(f_\eta; r_{\text{ref}}). \quad (17)$$

An expression for $\phi_3(f_\eta; r)$ is given in the Appendix.

The inverse range Fourier transform of (16), can be evaluated approximately by the method of stationary phase [22]. However, this is complicated by the cubic phase term, so to simplify the derivation an approximation is made to the stationary point, assuming that the cubic term is small enough that the following condition holds:

$$|Y_m| \ll \frac{1}{|2K_m KT|}. \quad (18)$$

That is, the signal is assumed to be dominantly linear FM, with a small nonlinear FM component. The range-Doppler domain representation of the filtered signal can then be shown to be

$$\begin{aligned} S_Y(f_\eta, \tau; r) = {} & H_{ac}(f_\eta; r) m \left[\frac{K_m}{K} (\tau - \tau_d) \right] \\ & \times \exp[-j\pi K_m (\tau - \tau_d)^2] \\ & \times \exp\left[-j \frac{2\pi}{3} Y_m K_m^3 (\tau - \tau_d)^3 \right]. \end{aligned} \quad (19)$$

Also, to model the range dependence of the range-frequency rate $K_m(f_\eta; r)$, it is assumed to vary linearly with the range-time from the reference trajectory:

$$K_m(f_\eta; r) \approx K_{m\text{ref}}(f_\eta) + K_s(f_\eta) \Delta\tau(f_\eta; r) \quad (20)$$

where $K_{m\text{ref}}(f_\eta)$ is the frequency rate at the reference range, and $K_s(f_\eta)$ is the slope of the variation.

The multiplication of the filtered signal by the chirp scaling phase function is described by

$$\begin{aligned} S_{Y\alpha}(f_\eta, \tau; r) = {} & S_Y(f_\eta, \tau; r) \\ & \times \exp\Big[-j\pi q_2(f_\eta)(\tau - \tau_{\text{ref}})^2 \\ & - j \frac{2\pi}{3} q_3(f_\eta)(\tau - \tau_{\text{ref}})^3 \Big]. \end{aligned} \quad (21)$$

The phase function at each range line is centered on the reference trajectory $\tau_{\text{ref}}(f_\eta)$ and has quadratic and cubic phase coefficients $q_2(f_\eta)$ and $q_3(f_\eta)$, respectively.

After chirp scaling, $S_{Y\alpha}(f_\eta, \tau; r)$ is Fourier transformed with respect to τ to get the SAR transfer function of the filtered, chirp scaled signal. Again, the phase of the SAR transfer function is expressed as a series in f_τ, where each coefficient is in turn expressed as a series in $\Delta\tau(f_\eta; r)$ in order to model its range dependence. The coefficient of the phase term that is linear in f_τ defines the range migration trajectory after chirp scaling, for a scatterer at range r. The expression for this scaled trajectory contains

linear and quadratic terms in $\Delta\tau(f_\eta;r)$ that depend on the signal and chirp scaling parameters: $K_{m\text{ref}}$, K_s, Y_m, q_2, and q_3. The terms of this scaled trajectory can be equated to those of the desired trajectory in (15), to remove the range dependence of RCMC. Next, the higher order phase terms in f_τ in the SAR transfer function correspond to range compression and SRC. In the coefficient of the quadratic term in f_τ, the range dependence is represented by a linear term in $\Delta\tau(f_\eta;r)$, which also depends on the signal and chirp scaling parameters mentioned above. Thus, to remove the range dependence of SRC it is required set this $\Delta\tau(f_\eta;r)$ term to zero. The above constraints result in a set of three equations in $q_2(f_\eta)$, $q_3(f_\eta)$, and $Y_m(f_\eta)$, which can be solved to give

$$\begin{aligned} q_2 &= K_{m\text{ref}}[\alpha_v - 1] \\ q_3 &= \frac{K_s(\alpha_v - 1)}{2} - \alpha_v^2 K_{m\text{ref}}\beta \\ Y_m &= \frac{K_s(\alpha_v - 0.5) - \alpha_v^2 K_{m\text{ref}}\beta}{K_{m\text{ref}}^3(\alpha_v - 1)}. \end{aligned} \tag{22}$$

The cubic phase filter coefficient $Y(f_\eta)$ is then found from $Y_m(f_\eta)$ and (17). Used together in the nonlinear FM filtering method, the processing coefficients $q_2(f_\eta)$, $q_3(f_\eta)$, and $Y(f_\eta)$ result in phase terms in the SAR transfer function, corresponding to bulk RCMC and SRC, which are range invariant. Thus, these phase terms can then be removed by a conjugate multiply in the two-dimensional frequency domain, performing accurate RCMC and SRC across the range swath in squint mode SAR. The phase of the range matched filter at this step is given by

$$\phi_{mf}(f_\eta, f_\tau) = \frac{\pi f_\tau^2}{\alpha_v K_{m\text{ref}}} + \frac{2\pi(q_3 + Y_m K_{m\text{ref}}^3) f_\tau^3}{3\alpha_v^3 K_{m\text{ref}}^3} \tag{23}$$

where the cubic term results from the cubic phase terms in the signal and the chirp scaling phase function.

After the range inverse FFT takes the data back to the range-Doppler domain, range-dependent azimuth compression is performed, and the phase correction factor is given by

$$\begin{aligned} \phi_\Delta(f_\eta;r) = &-\pi K_{m\text{ref}}\left(1 - \frac{1}{\alpha_v}\right)\Delta\tau(f_\eta;r)^2 \\ &- \left[\frac{\pi K_s}{3}\left(1 - \frac{1}{\alpha_v}\right) - \frac{2\pi}{3}K_{m\text{ref}}\beta(2 - \alpha_v)\right] \\ &\times \Delta\tau(f_\eta;r)^3. \end{aligned} \tag{24}$$

B. Limitations

The performance of nonlinear FM filtering method is eventually limited by the condition that is placed on the cubic phase filter coefficient in (18), and by a range-frequency shift of the signal that is introduced as a side-effect of chirp scaling. The range-frequency shift is given approximately by

$$\delta f_\tau = [\alpha_v(f_\eta) - 1]K_{m\text{ref}}(f_\eta)\Delta\tau(f_\eta;r) \tag{25}$$

and varies with the range of the scatterer. Thus, to avoid a loss of bandwidth when range matched filtering in the frequency domain, the maximum shift should be small enough to keep the range-frequency components of the signal less than the Nyquist rate. The range-frequency shift increases with the amount of scaling, and so increases with the azimuth-frequency offset of $f_{\eta r}$ from the azimuth-frequency band of the signal. However, in nonlinear FM chirp scaling, the reference azimuth-frequency must be outside of the azimuth-frequency band of the signal. This is because at $f_{\eta r}$ the scatterer trajectory and desired trajectory intersect, so at this range line there is no chirp scaling effect for the nonlinear FM component to interact with, and the desired effect of removing the range dependence of SRC cannot be obtained. This can also be seen from the expression for Y_m, which becomes very large as α_v approaches one. By substituting the expression for $Y_m(f_\eta)$ from (22) into (18) and making approximations, the condition on $Y_m(f_\eta)$ can be shown to imply the following constraint on $f_{\eta r}$:

$$|f_\eta - f_{\eta r}| \gg \left|\frac{KTf_{\eta r}}{f_0}\right|. \tag{26}$$

That is, in order to make use of the nonlinear FM component, there is a lower bound on the azimuth-frequency offset between $f_{\eta r}$ and the signal band. This results in a certain range-frequency shift due to chirp scaling, which is the price that must be paid in order to use nonlinear FM chirp scaling to accommodate the range dependence of SRC.

To determine the extent of the frequency shift in this case, $f_{\eta r}$ was chosen so that the offset to the azimuth-frequencies in the band was greater than twice the bound given in (26). This condition was used with the nonlinear FM filtering method in the simulations with good results. Then, the value of δf_τ was calculated at the edge of the swath for a spaceborne SAR with squint angles up to 40 deg for L-band and 50 deg for C-band. The maximum frequency shift was found to be less that ten percent of the range bandwidth. For typical oversampling rates of about twenty percent, this keeps the range-frequency components within the Nyquist rate, although some loss of bandwidth may occur due to frequency components taken outside of the window of the range matched filter.

C. Computation

The cost of the nonlinear FM filtering method is equal to the cost of the original chirp scaling

algorithm, plus the cost of the extra filtering step. The computation of the original chirp scaling algorithm can be compared with that of the standard range-Doppler algorithm, although range-Doppler is not as accurate at high squint. Alternatively, it can be compared with an extension of range-Doppler called the squint imaging mode algorithm, which accommodates the azimuth-frequency dependence of SRC but still requires an interpolator [7]. Chirp scaling is more efficient, in terms of computational requirement, since the interpolator for RCMC is replaced by the phase function multiply. For example, for a data block of 4096 by 4096 samples, chirp scaling requires about ten percent fewer multiplies than the range-Doppler or squint imaging mode algorithms with an eight point interpolator. Also, chirp scaling requires the same amount of memory as conventional algorithms: that is, enough to hold a range or azimuth line of the data block being processed. Another aspect of SAR processing is the corner turning of data on disk that is required to access lines of data in different directions. The chirp scaling algorithm, as with the squint imaging mode algorithm, requires two more corner turns than range-Doppler in order to perform azimuth-frequency dependent SRC.

The extra filtering step in the nonlinear FM filtering method requires a range FFT, multiply, and range inverse FFT above the cost of the original chirp scaling algorithm, although no extra corner turns are required. This step is used to remove the range-dependent SRC error. Thus, the extra computation in this step can be compared with that of another approach for achieving nearly the same accuracy: namely, a time-domain filter to perform residual range-dependent SRC. The extra computation of the time-domain filter approach depends on the length of the filter, as determined by the amount of compression error, and therefore depends on the squint angle. To make this comparison, Fig. 3 shows graphs of the number of complex multiplications versus the number of samples in a range line. Graphs are presented for L-band and C-band, and each case shows the results for the nonlinear FM filtering step, and the results for the time-domain filtering step for two different squint angles. At smaller squint the time domain filter requires less computation since the error is small and the filter is short. At high squint, the computation of the nonlinear FM filtering step is about half that of the time-domain filter. Also, the nonlinear FM filtering method requires only FFT and multiply operations, making it relatively straightforward to implement.

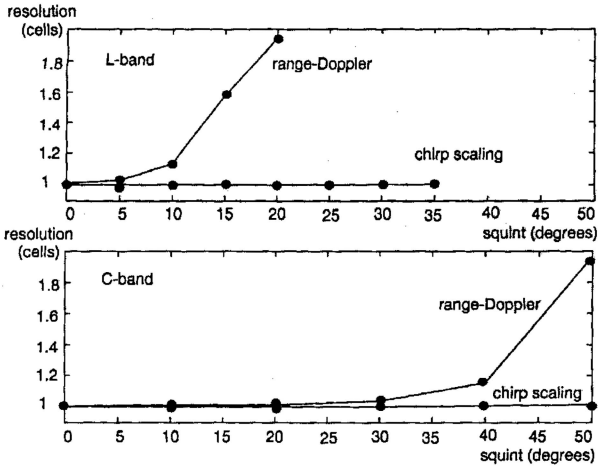

Fig. 3. Computation of time-domain SRC filter (t-d) versus frequency domain cubic phase filtering step (fft). Top: L-band SAR at squint angles of 20 and 40 deg. Bottom: C-band SAR at squint angles of 30 and 50 deg.

V. NONLINEAR FM PULSE METHOD

The nonlinear FM pulse method accommodates the range dependence of SRC approximately, without any increase in computation above that of the original chirp scaling algorithm. In this method, the nonlinear FM component is approximated by its value at the Doppler centroid and kept constant in azimuth-frequency. In this way, the required component can be incorporated directly into the transmitted pulse. This approach is feasible given digital signal generation and knowledge of the squint angle from the attitude control of the antenna. Thus, the nonlinear FM component is present in the received signal without the need of the filtering step. With the data collected with the nonlinear FM pulse, it is processed with the same operations as the original chirp scaling algorithm, although the values of phase function coefficients are those of the nonlinear FM filtering method described above.

To determine the required phase modulation of the transmitted pulse, (22) and (17) can be used to find the cubic phase filter coefficient at the Doppler centroid:

$$Y_c = Y_m(f_{\eta c}) - \frac{3\phi_3(f_{\eta c}; r_{\text{ref}})}{2\pi}. \tag{27}$$

Then, a received signal that is approximately the same as that achieved by the filtering step can be obtained with the following transmitted pulse:

$$p(\tau) = m(\tau)\exp\left[-j\pi K\tau^2 - j\frac{2\pi}{3}Y_c K^3\tau^3\right]. \tag{28}$$

The approximation of using a cubic phase coefficient that is constant in azimuth frequency has a negligible effect on RCMC. However, the ability to remove the range-dependent quadratic phase error is impaired at azimuth-frequencies other than the Doppler centroid. This results in a range-dependent phase error in the SAR transfer function, which is zero at the Doppler centroid and increases toward the edges of the

azimuth-frequency band. This phase error is given by

$$\phi_{\text{err}}(f_\eta, f_\tau; r) = -2\pi \frac{K_{m\text{ref}}(\alpha_v - 1)\Delta\tau(f_\eta; r)}{\alpha_v^3} \times (Y(f_\eta) - Y_c) f_\tau^2 \quad (29)$$

which can be shown to be approximately

$$\phi_{\text{err}}(f_\eta, f_\tau; r) \approx \frac{\pi K_s \Delta\tau(f_\eta; r)(f_\eta - f_{\eta c}) f_\tau^2}{\alpha_v^3 K_{m\text{ref}}(f_{\eta c} - f_{\eta r})}. \quad (30)$$

Note that because of the $(f_{\eta c} - f_{\eta r})$ term in the denominator, this error can be made to decrease by choosing a greater azimuth-frequency offset between the reference and the Doppler centroid. However, since the range-frequency shift due to chirp scaling increases with this offset, there is a tradeoff between the range-frequency shift and the focusing error.

In the nonlinear FM pulse method, the determination of the phase modulation of the transmitted pulse requires a knowledge of the Doppler centroid, which in turn requires an accurate knowledge of the squint angle. However, in spaceborne SAR, the antenna pointing direction can only be measured to within a degree or so, and a more accurate estimate of the Doppler centroid is obtained from the received data during processing [23]. Thus, the coefficient Y_c that is calculated for pulse transmission may not be the correct one, being calculated at some azimuth-frequency other than the Doppler centroid. This can have an effect on performance, but fortunately the processing can be modified in order to avoid an increase in the focusing error. To see how this can be done, note that Y_c depends on the initial reference azimuth-frequency, $f'_{\eta r}$, that was used in its calculation. However, the value of reference azimuth-frequency used during processing, $f_{\eta r}$, can be different. Thus, $f_{\eta r}$ can be chosen such that the cubic phase coefficient that was used in the transmitted pulse is equal to the one that is required for accurate processing.

The phase error in the SAR transfer function due to the approximation in this method, given in (29), can be interpreted as a quadratic phase error in range-frequency, that varies across the azimuth-frequency band. Thus, the resulting broadening of the range compressed pulses varies with azimuth-frequency, and after azimuth compression, this broadening is averaged to get an overall broadening in the range impulse response. This focusing error can be characterized by the maximum phase error in the SAR transfer function at the edge of the azimuth-frequency band, and to keep the overall broadening of the range impulse response to less five percent, this maximum phase error should be less than about 120 deg [6]. To investigate the effect of the approximation in the nonlinear FM pulse method, the range-frequency shift and the maximum phase error were calculated for spaceborne SAR parameters at

TABLE I
Range-Frequency Shift and Maximum Phase Error in Nonlinear FM Pulse Method, With ±1 Degree Squint Estimate Error

	L-band		C-band	
squint (degrees)	freq. shift (% of bandwidth)	maximum phase error (degrees)	freq. shift (% of bandwidth)	maximum phase error (degrees)
10	3.2	27.6	0.9	7.7
20	7.2	75.6	2.5	22.1
30	10.8	133.3	5.1	44.6
40	13.2	197.8	8.9	85.2
50	–	–	14.3	179.4

L-band and C-band, with a scatterer at the edge of the swath where $(r - r_{\text{ref}}) = 20$ km. The azimuth-frequency offset from $f_{\eta r}$ to the Doppler centroid was chosen to ensure that the minimum azimuth-frequency was four times the lower bound in (26). Also, a ±1 deg antenna pointing error was assumed in calculating the cubic phase coefficient of the transmitted pulse, and $f_{\eta r}$ was adjusted to accommodate this as described above. Table I shows the worst case frequency shift and phase error for different squint angles. The results are acceptable for all but the highest values of squint that are shown (40 deg for L-band and 50 deg for C-band). At this squint angle the phase error is large enough to cause a noticeable range broadening of the processed image of a point scatterer, and the range-frequency shift is over ten percent which is likely to cause some loss of bandwidth. However, even for this case the degradation is small compared with the effect of the range dependence of SRC.

VI. SIMULATIONS

To investigate the effect of approximations in the algorithms and the improvement with the new approach, data from a point scatterer was simulated using parameters from a spaceborne SAR such as Seasat or ERS-1, with squint angles up to 35 deg for L-band, and 50 deg for C-band. This data was processed with different algorithms, and the resulting complex image of a point scatterer was used to measure the 3 dB resolution width, sidelobe level, registration, and phase as indicators of performance. In the results presented here, resolution is measured in cells, where one cell is the minimum theoretical resolution width as determined by the signal bandwidth and the rectangular amplitude weighting of the spectrum. Also, only range resolution is presented since azimuth resolution was not as affected by approximations in the algorithms.

First, to compare chirp scaling with range-Doppler, the scatterer was placed at the reference range. Thus the results of the comparison show the effect of the

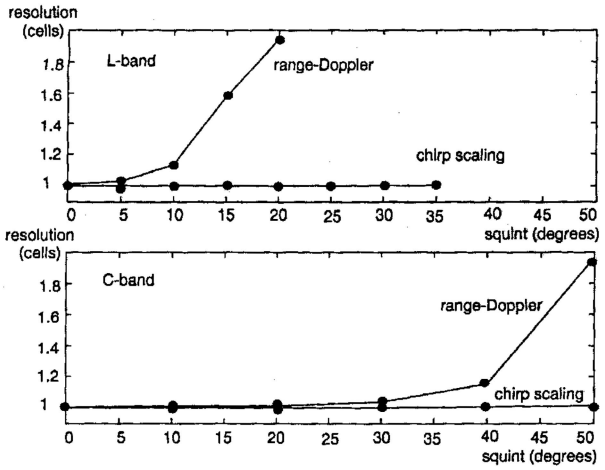

Fig. 4. Range resolution versus squint for range-Dopler and chirp scaling algorithms. Scatterer at reference range. Top: L-band. Bottom: C-band.

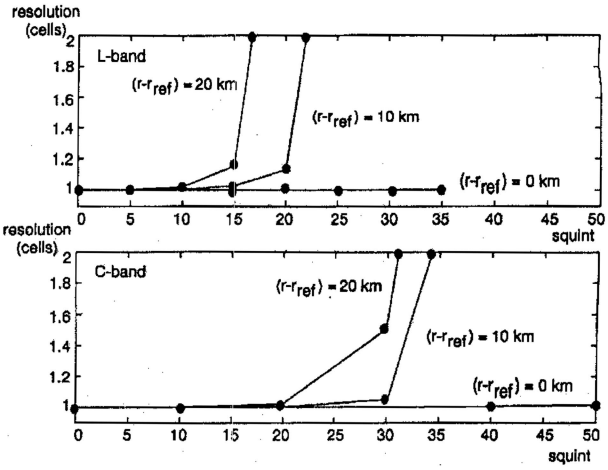

Fig. 5. Range resolution versus squint for chirp scaling algorithm with scatterer at different distances from reference range. Top: L-band. Bottom: C-band.

TABLE II
Maximum Sidelobe Level in Range Direction for Chirp Scaling Algorithm With Scatterer at Different Distances From Reference Range

	Maximum sidelobe level in range (dB)			
	L-band		C-band	
squint	$r - r_{ref} = 10km$	$r - r_{ref} = 20km$	$r - r_{ref} = 10km$	$r - r_{ref} = 20km$
0	-13.2	-13.2	-13.2	-13.2
10	-12.8	-11.7	-13.2	-13.1
20	-7.0	-0.3	-12.7	-11.3
30	–	–	-9.7	-3.5
40	–	–	-0.8	–

azimuth-frequency dependence of SRC. Fig. 4 shows the results of resolution versus squint angle. Since the scatterer is at the reference range in this case, the chirp scaling algorithm achieves the theoretical resolution width independently of squint angle. The approximation in the range-Doppler algorithm causes noticable resolution broadening for squint angles above about 5 deg for L-band and 30 deg for C-band.

Next, to investigate the approximation in the range dependence of SRC in the chirp scaling algorithm, the scatterer was placed at different distances from the reference range. Fig. 5 shows the results of range resolution versus squint angle for spaceborne SAR parameters at L-band and C-band, with the scatterer at 0 km, 10 km, and 20 km from the reference range. The results show a noticeable broadening of range resolution above 10 or 15 deg squint for L-band, and above 20 or 30 deg squint for C-band. Also, in each case resolution degrades rapidly above a certain squint angle. Next, Table II shows the range sidelobe level for the chirp scaling algorithm, in number of dB from the peak of the range impulse response. Since a rectangular weighting was used in the frequency domain, a value of -13.2 dB represents the theoretical sidelobe level of the sinc function. Blank entries of the table mean that the response was too distorted to provide adequate measurement. At L-band, the increase in sidelobe level becomes noticeable above about 10 deg squint, and for C-band the increase becomes noticeable above about 20 deg squint.

In order to verify the performance of the nonlinear FM chirp scaling approach, the point scatterer was placed at the edge of the swath, where $(r - r_{\text{ref}}) =$ 20 km. For the nonlinear FM filtering method, a linear FM pulse was used in simulating the point scatterer data. For the nonlinear FM pulse method, the transmitted pulse of (28) was used, where a ± 1 deg squint estimate error was assumed in calculating the nonlinear FM component. In each case, and the window of the range matched filter was thirteen percent wider than the range bandwidth of the signal. First, Fig. 6 illustrates the results at L-band and 25 deg squint by showing contour plots of the processed images of point scatterers, obtained with the different algorithms. As can be seen, the result of the original chirp scaling algorithm in this case suffers from severe broadening and distortion. The nonlinear FM filtering method achieves the two-dimensional sinc function corresponding to the rectangular weighting in the frequency domain, whereas the approximation in

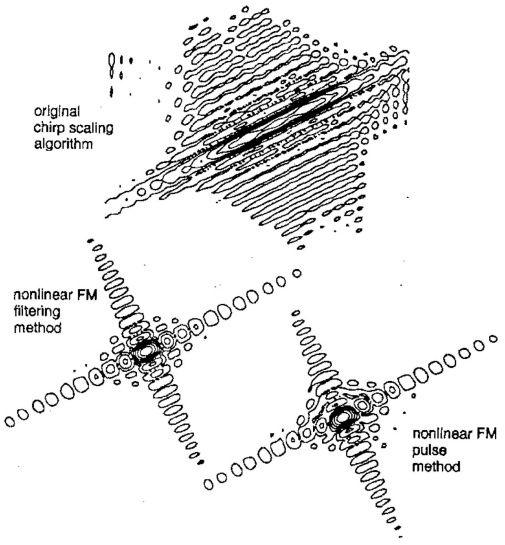

Fig. 6. Contour plots of processed images of points scatterers for L-band SAR data at 25° squint ($r - r_{ref}$) = 20 km, using original chirp scaling algorithm, nonlinear FM filtering method, and nonlinear FM pulse method.

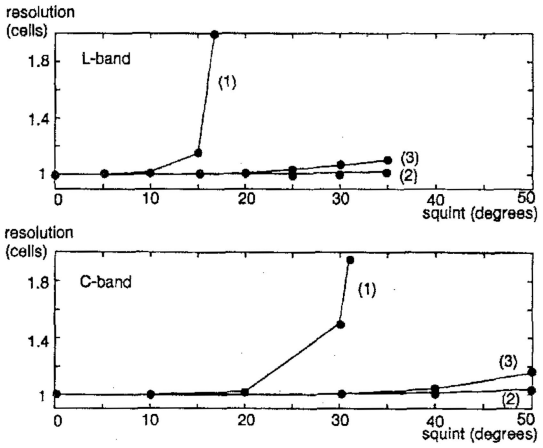

Fig. 7. Range resolution width in cells versus squint angle in degrees: (1) original chirp scaling algorithm; (2) nonlinear FM filtering method; (3) nonlinear FM pulse method.

the nonlinear FM pulse method causes some minor distortion in sidelobes. Next, Fig. 7 shows plots of range resolution width versus squint angle for the original chirp scaling algorithm, the nonlinear FM filtering method, and the nonlinear FM pulse method. The nonlinear FM filtering method achieves nearly the theoretically minimum resolution width of one cell, for squint angles up to 35 deg for L-band and 50 deg for C-band. The nonlinear FM pulse method achieves good performance up to smaller values of squint (about 30 deg for L-band and 40 deg for C-band). At higher squint angles the approximation in the pulse method causes resolution broadening of up to ten to twenty percent, but the performance is greatly improved over that of the original chirp scaling algorithm. The range sidelobe levels that result with the nonlinear FM filtering method and nonlinear FM

TABLE III
Maximum Sidelobe Level in Range Direction: Nonlinear FM Filtering Method and Nonlinear FM Pulse Method

	Maximum Sidelobe Level in Range (dB)			
	L-band		C-band	
squint	filtering method	pulse method	filtering method	pulse method
10	-13.2	-13.1	-13.2	-13.2
20	-13.2	-12.5	-13.2	-13.0
30	-12.8	-11.7	-13.2	-12.9
40	–	–	-13.2	-12.1
50	–	–	-13.1	-11.3

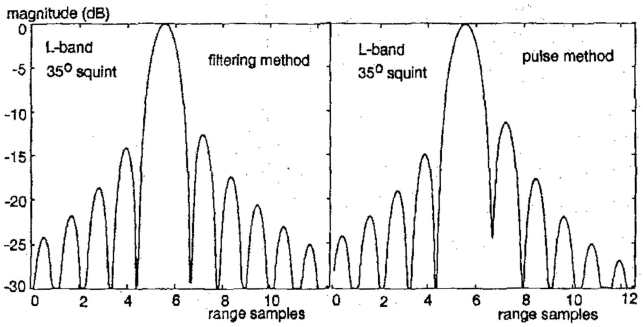

Fig. 8. Magnitude of range slice of processed image of point scatterer for L-band SAR data at 35° squint ($r - r_{ref}$) = 20 km, using nonlinear FM chirp scaling: filtering method and pulse method.

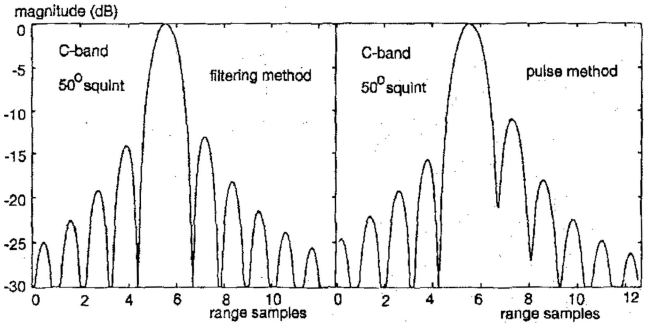

Fig. 9. Magnitude of range slice of processed image of point scatterer for C-band SAR data at 50° squint ($r - r_{ref}$) = 20 km, using nonlinear FM chirp scaling: filtering method and pulse method.

pulse method are shown in Table III for different squint angles, for the scatterer at ($r - r_{ref}$) = 20 km. The results are close to the −13.2 dB level of the sinc function, with at most a 2 dB degradation for the highest values of squint. This is a significant improvement over the results of the original chirp scaling algorithm in Table II. To illustrate the worst case shape of the processed image of the point scatterer in the range direction, Figs. 8 and 9 show the magnitude of the range impulse response for both methods, at 35 deg for L-band and 50 deg for C-band,

respectively. Again, in each case the nonlinear FM filtering method achieved nearly the theoretical shape of the *sinc* function, while the increase in sidelobe level due to the approximation in the nonlinear FM pulse method is evident.

In addition to resolution and sidelobe level, an error in the range registration of the image of a point scatterer can occur, due to an error in RCMC in the nonlinear FM chirp scaling algorithm. To verify the accuracy of RCMC in this approach, the range registration was measured for the different squint angles and wavelengths, for the two methods of nonlinear FM chirp scaling. For a scatterer at the edge of the swath, the worst case registration error was found to be 0.07 cells or less, which is negligible. Finally, the peak phase in the image of a point scatterer, which is used in advanced applications of SAR imagery such as interferometry, is very sensitive to processing errors. The approximations in the range-Doppler and original chirp scaling algorithms cause very large errors in the phase at high squint. In the simulation results of the nonlinear FM filtering method and the nonlinear FM pulse method, the worst case peak phase error at high squint at the edge of the swath was 5 deg, which is negligible.

VII. CONCLUSION

Image formation from squint mode, strip-map SAR has been limited by the range dependence of higher order coupling terms in the SAR transfer function phase, which imposes the requirement of space variant filtering in order to provide accurate focusing. The nonlinear FM chirp scaling approach presented in this paper is an extension of the chirp scaling algorithm, and provides accurate and efficient focusing of full swath, strip-map SAR data acquired with high squint angles. This is acheived by taking advantage of the interaction between a small nonlinear FM component of the signal, and the chirp scaling phase function. This effectively removes the range dependence of secondary range compression, allowing accurate processing to proceed in the two-dimensional frequency domain.

Two methods are proposed for implementing the new approach. Both methods give significantly improved performance in terms of range resolution and sidelobe level of the image of point scatterer, over the original chirp scaling algorithm for spaceborne SAR with squint angles above 10 deg for L-band and 20 deg for C-band. The nonlinear FM filtering method is the most accurate, but adds an extra filtering step to the chirp scaling algorithm. However, this method requires only FFT and multiply operations, and for high squint the extra processing step requires about half the computation of a time-domain filter approach to removing the residual SRC error. The method achieves nearly theoretical performance in terms of range resolution, sidelobe level, registration, and phase, for 40 km range swath and squint angles up to 35 deg for L-band and 50 deg for C-band. In the nonlinear FM pulse method, an approximation is made to the nonlinear FM component so that it can be incorporated directly into the transmitted pulse. In this way, the range dependence of SRC is accommodated with no extra computation above that of the original chirp scaling algorithm. The approximation in this method causes slightly poorer performance than the nonlinear FM filtering method. Nearly theoretical results are achieved for squint angles up to about 30 deg for L-band and 40 deg for C-band.

APPENDIX A. DEFINITIONS

Here, some expressions are given for some characteristics of the SAR signal. The quadratic coefficient of the phase of the SAR transfer function in (6) is given by

$$\phi_2(f_\eta;r) = \frac{\pi c r f_\eta^2}{2v_e^2(r)f_0^3\gamma^3(f_\eta;r)} \tag{31}$$

and the cubic coefficient is

$$\phi_3(f_\eta;r) = \frac{-\pi c r f_\eta^2}{2f_0^4 v_e^2(r)\gamma^5(f_\eta;r)}. \tag{32}$$

The variation of the effective velocity with range is modeled as an expansion of $v_e^2(r)$ about r_{ref}:

$$v_e^2(r) \approx \mathcal{V}_0 + \mathcal{V}_1(r - r_{\text{ref}}) + \mathcal{V}_2(r - r_{\text{ref}})^2 \tag{33}$$

where $\mathcal{V}_0$, $\mathcal{V}_1$, and $\mathcal{V}_2$ depend on orbital characteristics of the platform.

The range dependence of the range frequency rate, including SRC, is modeled by (20). The slope of the variation, in the case of a constant effective velocity, would be

$$K_{s0}(f_\eta) = -\frac{K_{m\text{ref}}^2(f_\eta)}{f_0}\frac{(1-\gamma^2(f_\eta;r_{\text{ref}}))}{\gamma^2(f_\eta;r_{\text{ref}})}. \tag{34}$$

To account for the effect of the range dependence of v_e on the range-frequency rate, the slope of the variation is modified as

$$K_s(f_\eta) = K_{s0}(f_\eta)\left[1 - \frac{r_{\text{ref}}\mathcal{V}_1}{\mathcal{V}_0\gamma^2(f_\eta;r_{\text{ref}}) - 0.5r_{\text{ref}}\mathcal{V}_1(1-\gamma^2(f_\eta;r_{\text{ref}}))}\right]. \tag{35}$$

APPENDIX B. DESIRED TRAJECTORY

In the extension of chirp scaling to account for a range-dependent effective velocity, a more accurate relationship between $\Delta\tau(f_{\eta r};r)$ and $\Delta\tau(f_\eta;r)$ is required than the one implied by (14). Using the model for the range variation of $v_e^2(r)$ in (33), the functions $\Delta\tau(f_\eta;r)$ and $\Delta\tau(f_{\eta r};r)$ can be expanded about r_{ref},

keeping terms up to the quadratic:

$$\begin{aligned}\Delta\tau(f_\eta;r) &\approx a(f_\eta)(r-r_{\text{ref}}) + b(f_\eta)(r-r_{\text{ref}})^2 \\ \Delta\tau(f_{\eta r};r) &\approx a(f_{\eta r})(r-r_{\text{ref}}) + b(f_{\eta r})(r-r_{\text{ref}})^2\end{aligned} \tag{36}$$

where the coefficients of the expansion are given by

$$\begin{aligned}a(f_\eta) &= \frac{2}{c\gamma(f_\eta;r_{\text{ref}})}\left[1-\frac{r_{\text{ref}}(1-\gamma^2(f_\eta;r_{\text{ref}}))\mathcal{V}_1}{2\gamma^2(f_\eta;r_{\text{ref}})\mathcal{V}_0}\right] \\ b(f_\eta) &= \frac{-(1-\gamma^2(f_\eta;r_{\text{ref}}))}{c\gamma^3(f_\eta;r_{\text{ref}})} \\ &\quad\times\left[\frac{\mathcal{V}_1}{\mathcal{V}_0}+\frac{r_{\text{ref}}\mathcal{V}_2}{\mathcal{V}_0}-\frac{r_{\text{ref}}\mathcal{V}_1^2}{\mathcal{V}_0^2}\left(1+\frac{3(1-\gamma^2(f_\eta;r_{\text{ref}}))}{4\gamma^2(f_\eta;r_{\text{ref}})}\right)\right].\end{aligned} \tag{37}$$

The first of the equations in (36) is used to find an approximate solution for $(r-r_{\text{ref}})$ in terms of $\Delta\tau(f_\eta;r)$, by assuming that $b(f_\eta) \ll a(f_\eta)$. Then, by substituting this solution into the second equation, and keeping terms up to the quadratic, a relationship between $\Delta\tau(f_\eta;r)$ and $\Delta\tau(f_{\eta r};r)$ is obtained which is used to represent the desired trajectory in (15). The scale factors in this equation are given by

$$\begin{aligned}\alpha_v(f_\eta) &= \frac{a(f_\eta)}{a(f_{\eta r})} \\ \beta(f_\eta) &= \frac{1}{a^2(f_\eta)}\left[b(f_{\eta r})-\frac{a(f_{\eta r})}{a(f_\eta)}b(f_\eta)\right].\end{aligned} \tag{38}$$

When v_e is constant so that $\mathcal{V}_1 = 0$ and $\mathcal{V}_2 = 0$, the scaling coefficients reduce to $\alpha_v(f_\eta) = \alpha(f_\eta)$ and $\beta(f_\eta) = 0$.

ACKNOWLEDGMENTS

We would like to thank Frank Wong for his comments.

REFERENCES

[1] Curlander, J. C., and McDonough, R. N. (1991)
Synthetic Aperture Radar: Systems and Signal Processing.
New York: Wiley, 1991.

[2] Way, J., and Smith, E. A. (1991)
The evolution of synthetic aperture radar systems and their progression to the EOS SAR.
IEEE Transactions on Geoscience and Remote Sensing, **29**, 6 (1991), 962–985.

[3] Cumming, I. G., and Bennett, J. R. (1979)
Digital processing of SEASAT SAR data.
In *ICASSP'79*, (1979), 710–718.

[4] Wu, C., Liu, K. Y., and Jin, M. (1982)
Modeling and a correlation algorithm for spaceborne SAR signals.
IEEE Transactions on Aerospace and Electronic Systems, **AES-18** (1982), 563–575.

[5] Jin, M. Y., and Wu, C. (1984)
A SAR correlation algorithm which accommodates large range migration.
IEEE Transactions on Geoscience and Remote Sensing, **GE-22**, 6 (1984), 592–597.

[6] Wong, F. H., and Cumming, I. G. (1989)
Error sensitivities of a secondary range compression algorithm for processing squinted satellite SAR data.
In *IGARSS'89 Proceedings*, (1989), 2584–2587.

[7] Chang, C. Y., and Jin, M., and Curlander, J. C. (1989)
Squint mode SAR processing algorithms.
In *IGARSS'89 Proceedings*, (1989), 1702–1706.

[8] Raney, R. K. (1992)
An exact wide field digital imaging algorithm.
International Journal of Remote Sensing, **13**, 5 (1992), 991–998.

[9] Cafforio, C., Prati, C., and Rocca, F. (1991)
SAR focusing using seismic migration techniques.
IEEE Transactions on Aerospace and Electronic Systems, **27**, 2 (1991), 194–207.

[10] Walker, J. L. (1980)
Range-Doppler imaging of rotating objects.
IEEE Transactions on Aerospace and Electronic Systems, **AES-16**, 1 (1980), 23–52.

[11] Ausherman, D. A., Kozma, A., Walker, J. L., Jones, H. M., and Poggio, E. C. (1984)
Developments in radar imaging.
IEEE Transactions on Aerospace and Electronic Systems, **AES-20**, 4 (1984), 363–398.

[12] Cumming, I. G., Wong, F. H., and Raney, R. K. (1992)
A SAR processing algorithm with no interpolation.
In *IGARSS'92 Proceedings*, (1992), 376–379.

[13] Runge, H., and Balmer (1992)
A novel high precision SAR focussing algorithm based on chirp scaling.
In *IGARSS'92 Proceedings*, (1992), 372–375.

[14] Raney, R. K., Runge, H., Balmer, R., Cumming, I. G., and Wong, F. H. (1994)
Precision SAR processing using chirp scaling.
IEEE Transactions on Geoscience and Remote Sensing, **32**, 4 (1994), 786–799.

[15] Raney, R. K. (1986)
Doppler properties of radars in circular orbits.
International Journal of Remote Sensing, **7**, 9 (1986), 1153–1162.

[16] Bamler, R. (1992)
A comparison of range-Doppler and wavenumber domain SAR focusing algorithms.
IEEE Transactions on Geoscience and Remote Sensing, **30**, 4 (1992), 706–713.

[17] Raney, R. K. (1992)
A new and fundamental Fourier transform pair.
In *IGARSS'92 Proceedings*, (1992), 106–107.

[18] Chang, C. Y., Jin, M. Y., and Curlander, J. C. (1992)
SAR processing based on the exact two-dimensional transfer function.
In *IGARSS'92 Proceedings*, (1992), 355–359.

[19] Raney, R. K., Cumming, I. G., and Wong, F. H. (1993)
Synthetic aperture radar processor to handle large squint with high phase and geometric accuracy.
U.S. Patent 5179383, 1993.

[20] Jin, M. Y., Hensley, S., and Chu, A. (1993)
Spaceborne SAR processing for wide beam and large squint angle systems.
In *SPIE Proceedings*, 1993.

[21] Wong, F. H., Cumming, I. G., and Raney, R. K. (1993)
Processing of simulated RADARSAT SAR data with squint by a high precision algorithm.
In *IGARSS'93 Proceedings*, 1993, 1176–1178.

[22] Papoulis, A. (1977)
Signal Analysis.
New York: McGraw-Hill, 1977.

[23] Li, F., Held, D. N., Curlander, J. C., and Wu, C. (1985)
Doppler parameter estimation for spaceborne synthetic-aperture radars.
IEEE Transactions on Geoscience and Remote Sensing, **GE-23**, 1 (1985), 47–55.

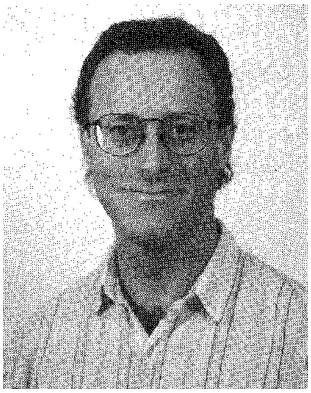

Gordon W. Davidson received the B.Sc. in electrical engineering from the University of Calgary in 1984, and the M.Eng. degree from Carleton University, Ottawa in 1986. He received the Ph.D. degree from the University of British Columbia, Vancouver, in 1994.

From 1986 to 1988 he worked at Bell Northern Research, Ottawa, Canada, in software development, and in 1989 he worked at Carleton University as a research assistant in the areas of echo cancellation, and equalization for the digital mobile radio channel. While a student he consulted for MacDonald Dettwiler, Richmond, Canada, in the area of SAR processing. He is currently a sessional lecturer in the Dept. of Electrical Engineering, University of British Columbia.

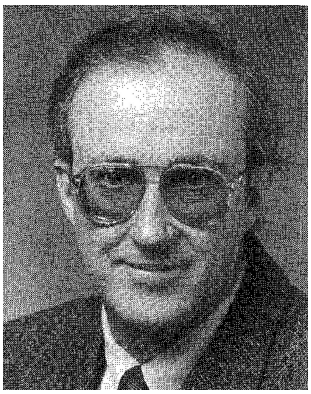

Ian Cumming received his B.Sc. in engineering physics at the University of Toronto in 1961, and a Ph.D. in computing and automation from Imperial College, University of London in 1968.

Following work in steel mill automation and sonar signal processing, he joined MacDonald Dettwiler and Associates in 1977. In 1993, Dr. Cumming joined the Department of Electrical Engineering at the University of British Columbia, where he holds the MacDonald Dettwiler/NSERC Industrial Research Chair in Radar Remote Sensing. The associated laboratory works in the fields of squinted SAR processing, satellite two-pass interferometry, airborne polarimetric radar classification, airborne interferometric radar geocoding, and SAR Doppler estimation.

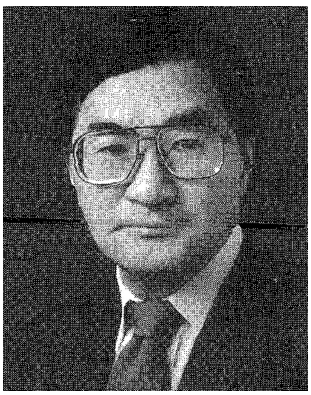

Mabo Robert Ito received the B.Sc. degree in engineering physics and the M.Sc. degree in electrical engineering from the University of Manitoba in 1960 and 1963, respectively, and the Ph.D. degree from the University of British Columbia in 1971.

From 1962 to 1966 and from 1970 to 1973, he was a research officer with the National Research Council of Canada. Since 1973, he has been with the Department of Electrical Engineering at the University of British Columbia where he is currently a professor. His research interests are in image and signal processing, pattern recognition, parallel processing, computer architecture and computer communication networks.